https://doi.org/10.1088/1361-648X/ab7ba2

Ligand substitution effects on the charge transport properties of the spin crossover complex $[Fe(Htrz)_{1+y-x}(trz)_{2-y}(NH_2trz)_x](BF_4)_y \cdot nH_2O$

Ion Soroceanu[1], Simona-Lacramioara Lupu[1], Ionela Rusu[1], Mario Piedrahita-Bello[2], Lionel Salmon[2], Gábor Molnár[2], Philippe Demont[3], Azzedine Bousseksou[2] and Aurelian Rotaru[1]

[1] Faculty of Electrical Engineering and Computer Science and MANSiD Research Center, Stefan cel Mare University, Suceava, Romania
[2] LCC, CNRS and Université de Toulouse, Toulouse, France
[3] CIRIMAT, CNRS and Université de Toulouse, Toulouse, France

E-mail: aurelian.rotaru@usm.ro and azzedine.bousseksou@lcc-toulouse.fr

Abstract

The complex dielectric permittivity of a series of spin crossover complexes, with variable ligand stoichiometry $[Fe(Htrz)_{1+y-x}(trz)_{2-y}(NH_2trz)_x](BF_4)_y \cdot nH_2O$, has been investigated as a function of temperature in a wide frequency range. In each compound, a substantial drop of the conductivity and permittivity is evidenced when going from the low spin to the high spin state, albeit with decreasing amplitude for increasing ligand substitution (i.e. for increasing x). The deconvolution of the dielectric spectra using the Havriliak–Negami equation allowed to extract the dipole and conductivity relaxation times, their distributions as well as the dielectric strengths in both spin states. Remarkably, no clear correlation appears between the conductivity changes and the lattice properties (Debye temperature) in the dilution series. We rationalize these results by considering the dimensionality of the system (1D), wherein the charge transport occurs most likely by hopping along the $[Fe(Rtrz)_3]_n^{n+}$ chains.

Keywords: spin crossover, charge transport properties, broad-band dielectric spectroscopy, phase transition, hysteresis, molecular switches

1. Introduction

Charge transport and dielectric properties of molecular spin crossover (SCO) complexes [1–4] have received recently increasing attention in view of their possible use in resistance and/or capacitance switching electronic components [5–9]. In particular, the electrical properties of the SCO compound $[Fe(Htrz)_2(trz)](BF_4)$ (trz = 1,2,4-triazolato) have been extensively investigated in its micro/nano-crystalline powder form as well as in various simple micro/nanoelectronic devices [10–24]. This compound exhibits a robust spin transition between the diamagnetic low spin ($t_{2g}^6e_g^0$) and paramagnetic high spin ($t_{2g}^4e_g^2$) configurations of the Fe(II) ions, which occurs above room temperature with a large thermal hysteresis loop [25]. Its structure consists of cationic chains of $[Fe(Htrz)_2(trz)]_n^{n+}$ (figure 1), whereas the BF_4^- counter-anions are located between the chains. Each chain is surrounded by six others, which are inter-connected through hydrogen bonds [26].

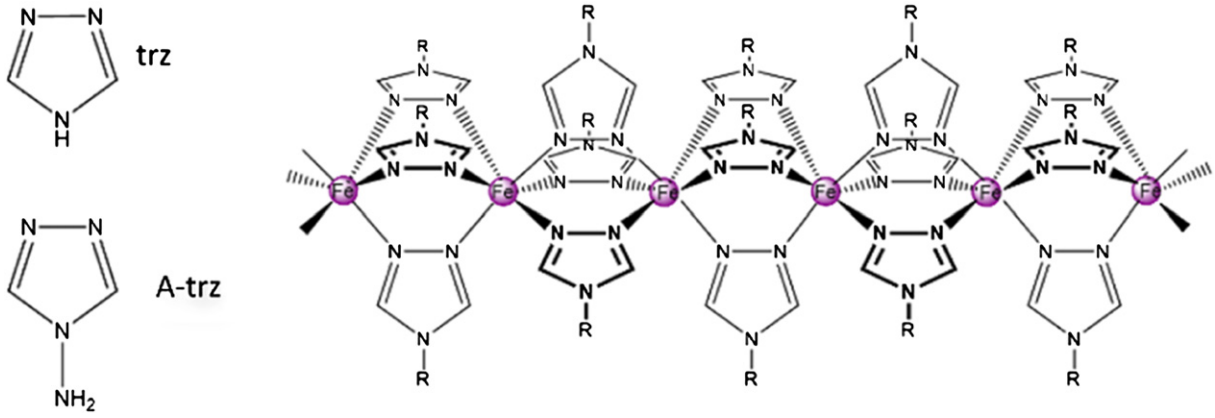

Figure 1. The ligands 1,2,4,4-*R*-triazole and schematic structure of the $[Fe(Rtrz)_3]_n$ chain.

In the past few years, we have shown that both the thermal [11] and pressure-induced [12] spin transitions in the bulk powder of $[Fe(Htrz)_2(trz)](BF_4)$ are accompanied by a substantial variation (up to three orders of magnitude) of the electrical conductivity, the low spin (LS) form being systematically more conducting than the high spin (HS) counterpart. Broadband dielectric spectroscopic investigations [13, 14] pointed out a clear link between the spin-state dependence of the dielectric relaxation frequencies and that of the conductivity. We suggested therefore that the the primary origin of the conductivity drop in the HS state is the global downshift of charge hopping (i.e. phonon) frequencies when going from the LS to the HS state. Remarkably, the room temperature conductance of $[Fe_{1-x}Zn_x(Htrz)_2(trz)](BF_4)$ solid solutions dropped by seven orders of magnitude for a ca 43% substitution of the open shell ($3d^6$) Fe(II) ions by closed shell ($3d^{10}$) Zn(II) ions [15]. This result indicates that the iron atoms are directly involved in the hopping charge transport, which can—in part—explain also the relatively large variation of the conductivity upon the SCO in this compound.

Recently, we have embarked in the study of a series of samples, derived from $[Fe(Htrz)_2(trz)](BF_4)$, wherein the triazole ligands have been partially replaced by the amino-substituted 1,2,4-4-NH_2-triazole (Atrz) ligand, leading to the 'molecular alloys' of general formulae $[Fe(Htrz)_{1+y-x}(trz)_{2-y}(Atrz)_x](BF_4)_y \cdot nH_2O$ [27]. The initial aim was to fine-tune the spin transition temperature, which indeed decreased by ca 30 K for $x = 0.3$. In addition, we revealed also a brusque variation of the structure of the compound, even for a small (ca 3.3%) degree of ligand substitution. Remarkably, this structural change gave rise to a pronounced decrease of the lattice cohesion as inferred from the drop of the Mössbauer–Debye temperature. The lattice softening in the ligand-diluted compounds could be associated with the acoustic part of the phonon density of states (PDOS), whereas the optical modes remained unaltered on the whole.

In the present paper, we report a broadband dielectric spectroscopic study of these ligand-substituted derviatives of $[Fe(Htrz)_2(trz)](BF_4)$. Owing to the drastic changes of their lattice properties, these compounds appear very appealing to investigate the links between charge transport, dielectric and lattice dynamical properties in a series of closely related compounds with very similar molecular structure.

2. Experimental details

The synthesis and physico-chemical characterization of the nanocristalline powder samples have been described in reference [27]. The complex impedance of the samples (pressed between stainless steel electrodes in a Teflon cylinder) was measured in a four-wire arrangement using a dielectric analyzer alpha-A combined with the impedance interface ZG4 (novocontrol technologies GmbH & Co. KG, Germany). Frequency sweeps were carried out from 0.1 Hz to 1 MHz at fixed temperatures with an AC amplitude of 1 V. The temperature was continously changed with a rate of ± 0.5 K min^{-1} between 293 K and 403 K. Magnetic measurements were performed using a MPMS3 SQUID magnetometer (Quantum Design Inc.), in DC mode, under a magnetic field of 1000 Oe, with a temperature rate of 2 K min^{-1}. Data were corrected for the diamagnetic contributions.

3. Results and discussion

Overall four 'mixed-ligand' powder samples were investigated with the following compositions (see [27] for more details on sample characterization and properties):

$$[Fe(Htrz)_2(trz)](BF_4) \cdot 0.7H_2O, \quad (1)$$

$$[Fe(Htrz)_{2.1}(trz)_{0.8}(Atrz)_{0.1}](BF_4)_{1.2} \cdot 0.8H_2O, \quad (2)$$

$$[Fe(Htrz)_{2.05}(trz)_{0.75}(Atrz)_{0.2}](BF_4)_{1.25} \cdot 0.85H_2O, \quad (3)$$

$$[Fe(Htrz)_2(trz)_{0.7}(Atrz)_{0.3}](BF_4)_{1.3} \cdot 0.95H_2O. \quad (4)$$

The sample morphologies are similar: they consist of nanoparticles with a mean size of ca 60 nm and a broad size distribution (± 30 nm).

The magnetic properties of the samples are summarized in figure 2(a), which shows the molar magnetic susceptibility $\times$ temperature product (χT) as a

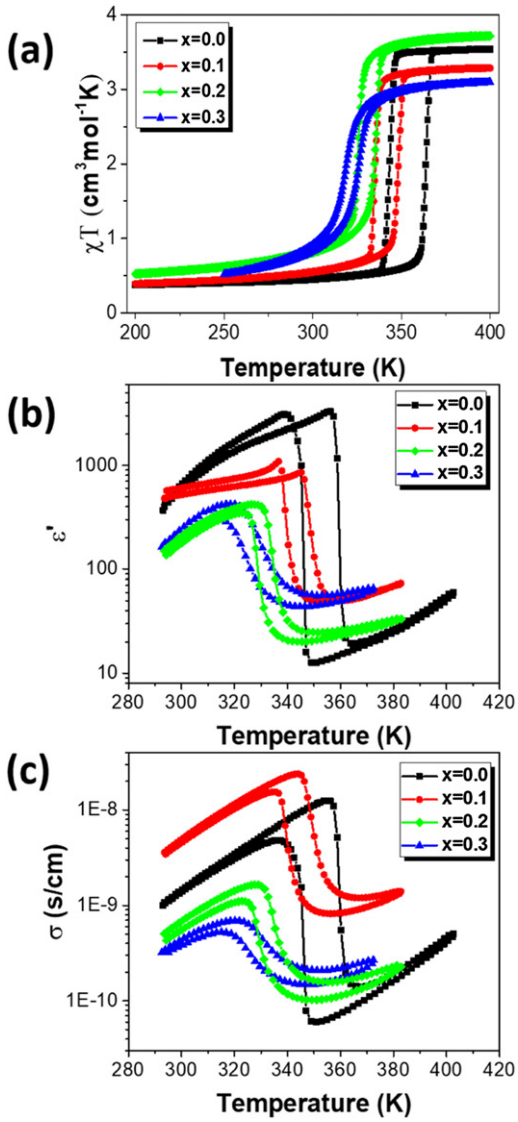

Figure 2. Temperature dependence of (a) the magnetic susceptibility × temperature product χT, (b) the real part of the dielectric permittivity (at 1 Hz) and (c) the real part of the AC conductivity (at 1 Hz) for compounds **1**–**4** on heating and cooling.

function of the temperature both on heating and cooling. In agreement with our previous measurements [27], each sample displays a spin transition above room temprature with hysteresis. However, for increasing amounts of Atrz ligands (i.e. for increasing values of x) the transition temperature progressively downshifts, the hysteresis width decreases and the transition becomes less abrupt. The low- and high-temperature χT values indicate a virtually complete spin transition between the LS ($S = 0$) and HS ($S = 2$) forms for each sample. It is important to note, however, that the variation of the HS fraction, which corresponds to the hysteresis region becomes significantly reduced in the dilution series (from ∼100% for $x = 0$ to ∼70% for $x = 0.3$). Figures 2(b) and (c) display, respectively, the temperature dependence of the real part of the dielectric permittivity (ε') and the real part of the AC conductivity (σ') acquired at 1 Hz for the four samples. (The temperature dependence of ε' and σ' recorded at

Table 1. Pre-exponential factors and activation energies of the ac conductivity (1 Hz) in the LS and HS states

Sample	σ_0^{HS} (S cm^{-1})	σ_0^{LS} (S cm^{-1})	E_a^{HS} (eV)	E_a^{LS} (eV)
1	8.4×10^{-3}	2.6×10^{-3}	0.58	0.37
2	1.6×10^{-5}	3.0×10^{-3}	0.31	0.34
3	6.2×10^{-6}	1.2×10^{-4}	0.34	0.31
4	1.4×10^{-5}	1.3×10^{-5}	0.35	0.27

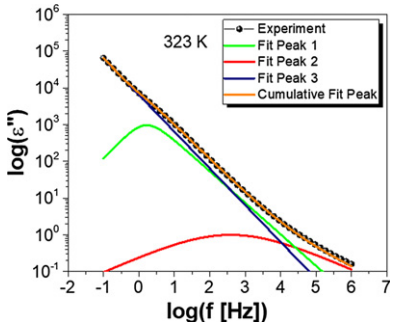

Figure 3. Representative dielectric spectrum of sample **1** (323 K) and its deconvolution using three HN functions. Peaks 1–3 correspond to a dipole relaxation, charge transfer relaxation and electrode/interface polarisation processes, respectively.

1 kHz and 0.1 MHz are shown in the ESI in figure S1 (https://stacks.iop.org/JPhysCM/32/264002/mmedia)). In agreement with our previous results on the bulk powder $[Fe(Htrz)_2(trz)](BF_4)$ [11–14], the nanocrystalline sample **1** exhibits a marked drop of both ε' and σ' when going from the low temperature (LS) to the high temperature (HS) phase. Both quantities change by ca three orders of magnitude, which is comparable with the published values for other $[Fe(Htrz)_2(trz)](BF_4)$ samples and is the highest for any reported SCO compound. (N.B. As it was discussed in reference [11], the specific sample preparation details lead to different morphologies, cristallinity and defects, which can considerably alter the amplitude of switching even for nominally the same compounds.) When increeasing the amount of Atrz ligands, the permittivity and conductivity changes associated with the SCO ($\Delta\varepsilon'_{HL}$ and $\Delta\sigma'_{HL}$) become progressively smaller. We shall note here the lack of any brusque change in the electrical behavior betweeen the 'parent sample' ($x = 0$) and the 'first dilution' ($x = 0.1$). This result strongly contrasts the previously reported drastic decrease of the Mössbauer–Debye temperature ($\theta_D^{x=0} = 285\,K$, $\theta_D^{x=0.1} = 226\,K$) between these two compounds. In other words, the structural change and associated lattice softening of the Atrz diluted samples is not reflected in the electrical properties.

The thermal activation energy of the electrical conductivity in the two spin states was determined for each sample using the Arrhenius equation:

$$\sigma = \sigma_0 e^{-\frac{E_a}{k_B T}}$$

where σ_0 is the pre-exponential factor, E_a is the thermal activation energy and k_B is the Boltzmann constant. Table 1 gathers the fit values for 1 Hz applied frequency. (Similar results

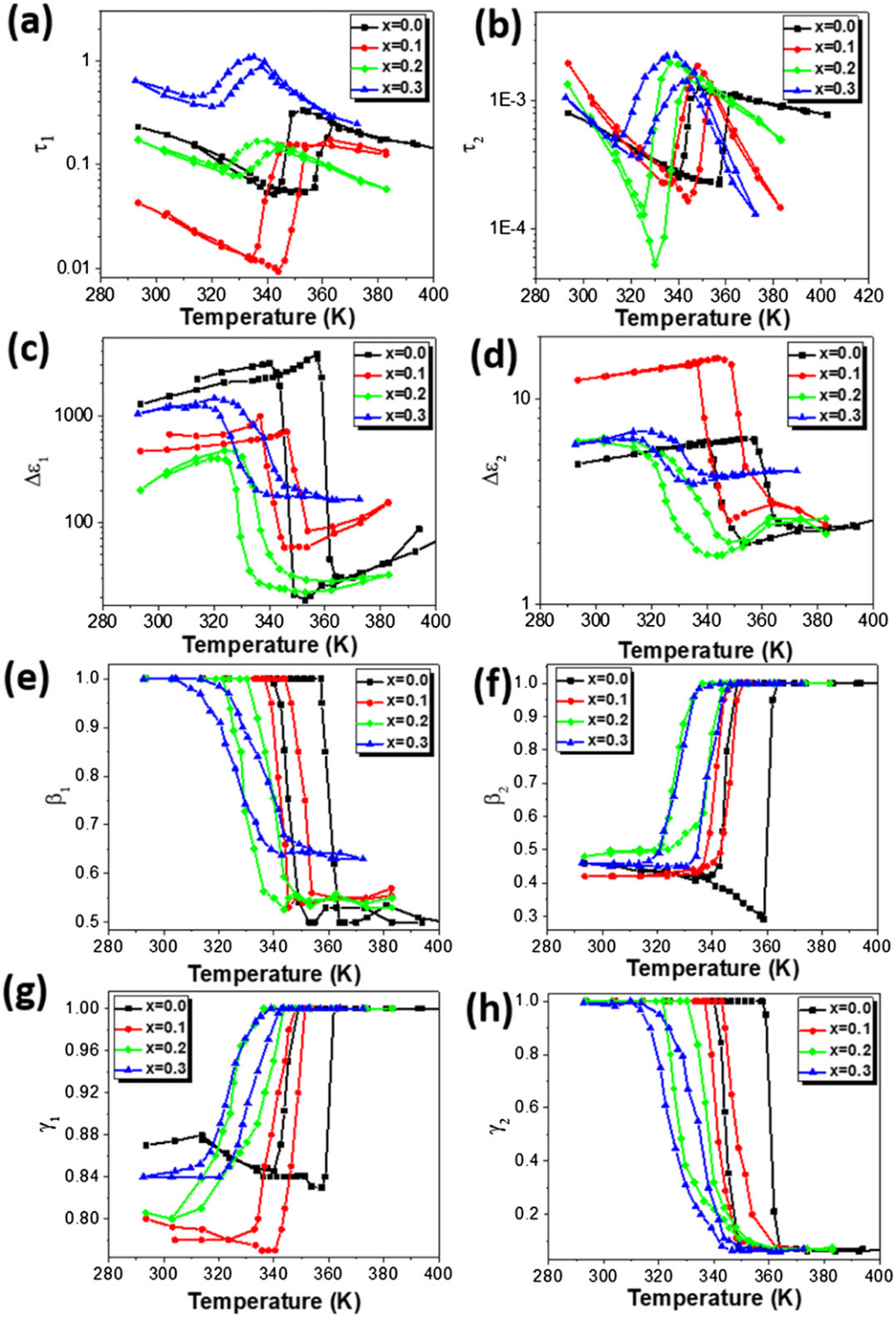

Figure 4. Temperature dependence of the Havriliak–Negami fitting parameters, which characterize the dipolar relaxation process (left column) and the charge transport relaxation process (right column).

were obtained at 1 kHz, which are shown in the ESI.) For the 'parent sample' **1** the thermal activation energy increases from 0.31 eV to 0.58 eV when going from the LS to the HS state, while for the other compounds (**2**–**4**) the activation energies remain similar (ca 0.3 eV) independently of the spin state of the compound. On the other hand, the values of the pre-exponential factors scatter more.

Although the temperature dependence of the complex permittivity (or conductivity) provides useful information on the charge carrier motion in molecular solids, a deeper insight

can be obtained from the analysis of its frequency dependence. Indeed, the movement of charge carriers in low-mobility solids (such as samples **1**–**4**) can be seen as a series of rapid hops between localized sites (potential energy wells) [28]. Since the carriers polarize the surrounding lattice, their hopping is associated with a structural relaxation. The concomitant movement of the charge carrier and the polarization cloud gives rise to a characteristic electrical relaxation frequency, which can be readily assessed from dielectric relaxation studies [29]. We have recently used this approach for the investigation of a bulk powder of $[Fe(Htrz)_2(trz)](BF_4)$ [14]. The phenomenological Havriliak–Negami (HN) equation [30] was employed to fit the frequency dependence of the complex dielectric permittivity. This analysis revealed three dielectric relaxation processes, which were attributed to electrode/interface polarization, dipole orientation and charge transport phenomena.

Using the same methodology we could obtain consistent fits for the dielectric spectra of samples **1**–**4** at various temperatures in the LS and HS states. As an example, figure 3 shows the frequency dependence of $\log(\varepsilon'')$ acquired at 323 K and the fitted dielectric relaxation peaks. (See figures S2–S5 in the ESI for the fitted data of the four samples at various temperatures, including both the real and imaginary parts of the permittivity.)

In the frame of the HN approach [30], the complex dielectric permittivity ($\varepsilon^* = \varepsilon' - i\varepsilon''$) is expressed as a function of the angular frequency (ω) of the applied electric field as:

$$\varepsilon^* = \varepsilon_\infty + \Delta\varepsilon/(1 + (i\omega t)^\beta)^\gamma$$

The model parameters are the dielectric strength $\Delta\varepsilon = \varepsilon_s - \varepsilon_\infty$ (where ε_s and ε_∞ stand for the permittivity in the low and high frequency limits, respectively), the dielectric relaxation time τ and the so-called shape parameters β and γ. The latter describe the symmetric and asymmetric broadening of the relaxation time distribution, respectively. The analysis of temperature dependence of the relaxation times—by introducing for example the Arrhenius relationship—reveals the energy barriers associated with the relaxation process. The obtained fit parameters for the dipole and charge transfer relaxations in samples **1**–**4** are summarized in figure 4. First, we shall note that the fit parameter values and their spin-state dependences observed for sample **1** are directly comparable with the fitted values reported in reference [14] for the bulk powder. This close correspondence between two samples synthesized in different conditions provides strong confidence for the validity of our analysis. The only notable difference appears in the dielectric strength associated with the dipole relaxation ($\Delta\varepsilon_1$), which is significantly higher for the present sample (ca 1000 vs 10). This difference might be linked to the difference in particle size (interfacial properties, defects, ...) or to the presence of water molecules in the nanocrystalline sample **1**.

Second, both the absolute values and the spin state dependence of the fitted parameters appear very similar for the the whole series of diluted samples **1**–**4**. Notably, the switching from the LS to the HS state leads systematically to an increase of the relaxation times and to a decrease of the dielectric strength for each sample and for both relaxation processes. In the case of the shape parameters the samples behave also in a comparable manner: for the dipole (resp. conductivity) relaxation the LS state is characterized by an asymmetric (resp. symmetric broadening) of the relaxation time distribution, whereas in the HS state the trend is exactly the opposite.

The analysis of the dielectric relaxations does not point thus to any systematic change of the dielectric properties in the dilution series we investigated. This finding contrasts with the progressive shrinking of the switching amplitude ($\Delta\varepsilon'_{SCO} = \varepsilon'_{LS} - \varepsilon'_{HS}$ and $\Delta\sigma'_{SCO} = \sigma'_{LS} - \sigma'_{HS}$) when increasing the value of x (figure 2). We believe that this reduced switching amplitude is related actually to the systematic variation of the spin transition properties in the dilution series. Indeed, we can see a close correspondence between the magnetic properties (figure 2(a)) and the electrical properties (figures 2(b) and (c)) of the samples. As mentionned above, the proportion of molecules, which show SCO *in the hysteresis region* becomes reduced along the dilution series, which obviously leads to reduced values of $\Delta\sigma'_{SCO}$ and $\Delta\varepsilon'_{SCO}$ in this temperature range. This can be also seen as the smearing out of the electrical response when the spin transition becomes more and more gradual. In addition, the spin transition is shifted to lower temperature for increasing dilution. Hence, the less efficient thermal activation may also contribute to the smaller switchig amplitudes.

4. Conclusions

We have investigated the effect of ligand substitution on the charge transport and dielectric properties in the $[Fe(Htrz)_{1+y-x}(trz)_{2-y}(Atrz)_x](BF_4)_y \cdot nH_2O$ (x = 0, 0.1, 0.2, 0.3) series of spin crossover compounds.

We have found that the softening of the crystal lattice (demonstrated in [27]) does not entail any remarkable effect on the macroscopic electrical properties of $[Fe(Htrz)_2(trz)](BF_4)$. This means that the electron–phonon coupling at the origin of the hopping charge transport must involve primarily optical modes of the coordination chain $[Fe(Htrz)_2(trz)]_n^{n+}$. This result comes to support our previous hypothesis [15] that the charge transport in this compound takes place primarily by carrier hopping between the iron ions along the chains. All these results point thus to the importance of the dimensionality (1D) of this compound in the charge transport properties. To verify this hypothesis it would be interesting to conduct electrical measurements on oriented single crystals.

Another finding concerns the progressive shrinking of the HS–LS switching amplitude of the permittivity and conductivity for increasing ligand dilution. This result could not be correlated with any change in the dielectric behavior of the samples and has been therefore associated with the progressive change of the spin crossover properties. Notably, it appears that the more gradual nature of the SCO in the diluted samples as well as the lower transition temperatures both tend to amalgamate the effect of the SCO with that of ordinary thermal activation on the electrical properties.

Future work should focus increasingly on the dielectric relaxation process in spin crossover solids and devices as they bring into light mechanistic aspects of charge transport phenomena. The open questions concern why in some cases the HS or the LS state is more conducting [11, 31] and how to increase/overcome the intrinsicaly low conductivity of SCO materials. The synthesis of conducting SCO materials and/or device engineering may be considered to this aim [5].

Acknowledgments

This work was founded by the European Commission through the SPINSWITCH project (H2020-MSCA-RISE-2016, Grant Agreement No. 734322). The PhD grant of MPB was financed by the Federal Univeristy of Toulouse and the Occitanie Region. The financial support of the EXCALIBUR project (Contract No. 18 PFE/16.10.2018) is also acknowledged.

ORCID iDs

Gábor Molnár https://orcid.org/0000-0001-6032-6393
Aurelian Rotaru https://orcid.org/0000-0002-8782-7988

References

[1] Gütlich P, Hauser A and Spiering H 1994 *Angew. Chem., Int. Ed.* **33** 2024
[2] Gütlich P and Goodwin H A ed 2004 *Spin Crossover in Transition Metal Compounds I–III* (Topics in Current Chemistry) (Berlin: Springer)
[3] Halcrow M A ed 2013 *Spin-Crossover Materials: Properties and Applications* (Oxford: Wiley)
[4] Bousseksou A ed 2018 *Spin Crossover Phenomenon* (Compte Rendus Chimie) (Amsterdam: Elsevier)
[5] Lefter C, Davesne V, Salmon L, Molnár G, Demont P, Rotaru A and Bousseksou A 2016 *Magnetochemistry* **2** 1
[6] Bellec A, Lagoute J and Repain V 2018 *C. R. Chim.* **21** 1287
[7] Ruiz E 2014 *Phys. Chem. Chem. Phys.* **16** 14
[8] Molnar G, Rat S, Salmon L, Nicolazzi W and Bousseksou A 2018 *Adv. Mater.* **30** 17003862
[9] Kumar K S and Ruben M 2017 *Coord. Chem. Rev.* **346** 176
[10] Prins F, Monrabal-Capilla M, Osorio E A, Coronado E and van der Zant H S J 2011 *Adv. Mater.* **23** 1545
[11] Rotaru A, Gural'skiy I A, Molnar G, Salmon L, Demont P and Bousseksou A 2012 *Chem. Commun.* **48** 4163
[12] Diaconu A, Lupu S L, Rusu I, Risca I M, Salmon L, Molnár G, Bousseksou A, Demont P and Rotaru A 2017 *J. Phys. Chem. Lett.* **8** 3147
[13] Lefter C, Gural'skiy I A, Peng H, Molnár G, Salmon L, Rotaru A, Bousseksou A and Demont P 2014 *Phys. Status Solidi* **8** 191
[14] Soroceanu I, Graur A, Coca E, Salmon L, Molnar G, Demont P, Bousseksou A and Rotaru A 2019 *J. Phys. Chem. Lett.* **10** 7391
[15] Lefter C, Tricard S, Peng H, Molnár G, Salmon L, Demont P, Rotaru A and Bousseksou A 2015 *J. Phys. Chem.* C **119** 8522
[16] Dugay J, Aarts M, Giménez-Marqués M, Kozlova T, Zandbergen H W, Coronado E and van der Zant H S J 2016 *Nano Lett.* **17** 186
[17] Dugay J, Evers W, Torres-Cavanillas R, Giménez-Marqués M, Coronado E and Van der Zant H S J 2018 *J. Phys. Chem. Lett.* **9** 5672
[18] Lefter C, Tan R, Dugay J, Tricard S, Molnar G, Salmon L, Carrey J, Rotaru A and Bousseksou A 2015 *Phys. Chem. Chem. Phys.* **17** 5151
[19] Lefter C, Tan R, Dugay J, Tricard S, Molnár G, Salmon L, Carrey J, Nicolazzi W, Rotaru A and Bousseksou A 2016 *Chem. Phys. Lett.* **644** 138
[20] Holovchenko A, Dugay J, Gimenez-Marques M, Torres-Cavanillas R, Coronado E and van der Zant H S J 2016 *Adv. Mater.* **28** 7228
[21] Koo Y S and Galán-Mascarós J R 2014 *Adv. Mater.* **26** 6785
[22] Rotaru A, Dugay J, Tan R P, Gural'skiy I A, Salmon L, Demont P, Carrey J, Molnar G, Respaud M and Bousseksou A 2013 *Adv. Mater.* **25** 1745
[23] Torres-Cavanillas R, Sanchis-Gual R, Dugay J, Coronado-Puchau M, Gimenez-Marques M and Coronado E 2019 *Adv. Mater.* **31** 1900039
[24] Lefter C, Tan R, Tricard S, Dugay J, Molnár G, Salmon L, Carrey J, Rotaru A and Bousseksou A 2015 *Polyhedron* **102** 434
[25] Kroeber J, Audiere J P, Claude R, Codjovi E, Kahn O, Haasnoot J G, Groliere F, Jay C and Bousseksou A 1994 *Chem. Mater.* **6** 1404
[26] Grosjean A, Négrier P, Bordet P, Etrillard C, Mondieig D, Pechev S, Lebraud E, Létard J F and Guionneau P 2013 *Eur. J. Inorg. Chem.* **2013** 796
[27] Piedrahita-Bello M, Ridier K, Mikolasek M, Molnar G, Nicolazzi W, Salmon L and Bousseksou A 2019 *Chem. Commun.* **55** 4769
[28] Austin I G and Mott N F 1969 *Adv. Phys.* **18** 41
[29] Kremer F and Schönhals A ed 2003 *Broadband Dielectric Spectroscopy* (Berlin: Springer)
[30] Havriliak S and Negami S 1967 *Polymer* **8** 161
[31] Molnár G, Cobo S, Vertelman E J M, Mahfoud T, van Koningsbruggen P J, Demont P and Bousseksou A 2009 *J. Phys. Chem.* C **113** 2586

Supporting Information

Ligand Substitution Effects on the Charge Transport Properties of the Spin Crossover Complex $[Fe(Htrz)_{1+y-x}(trz)_{2-y}(NH_2trz)_x](BF_4)_y \cdot nH_2O$

Ion Soroceanu,[1] Simona-Lacramioara Lupu,[1] Ionela Rusu,[1] Mario Piedrahita-Bello,[2] Lionel Salmon,[2] Gábor Molnár,[2] Philippe Demont,[3] Azzedine Bousseksou[2,*] and Aurelian Rotaru[1,*]

[1] *Faculty of Electrical Engineering and Computer Science and MANSiD Research Center, Stefan cel Mare University, Suceava, Romania*

[2] *LCC, CNRS and Université de Toulouse, Toulouse, France*

[3] *CIRIMAT, CNRS and Université de Toulouse, Toulouse, France*

E-mail: aurelian.rotaru@usm.ro and azzedine.bousseksou@lcc-toulouse.fr

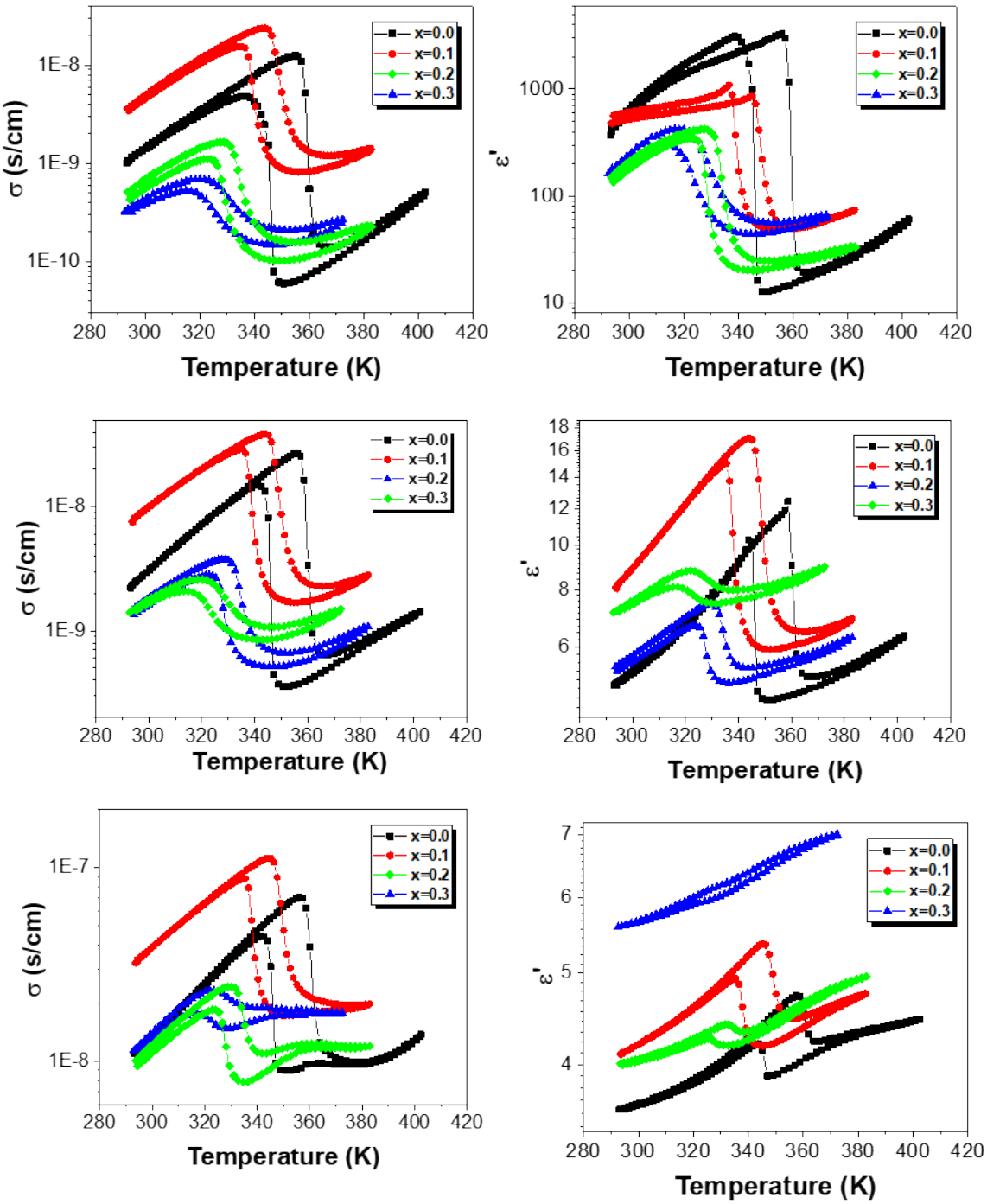

Figure S1. Temperature dependence of the real part of the ac conductivity (left column) and the real part of the dielectric permittivity (right column) for compounds **1-4** on heating and cooling. Top row: 1 Hz, middle row: 1 kHz, bottom row: 0.1 MHz applied frequency.

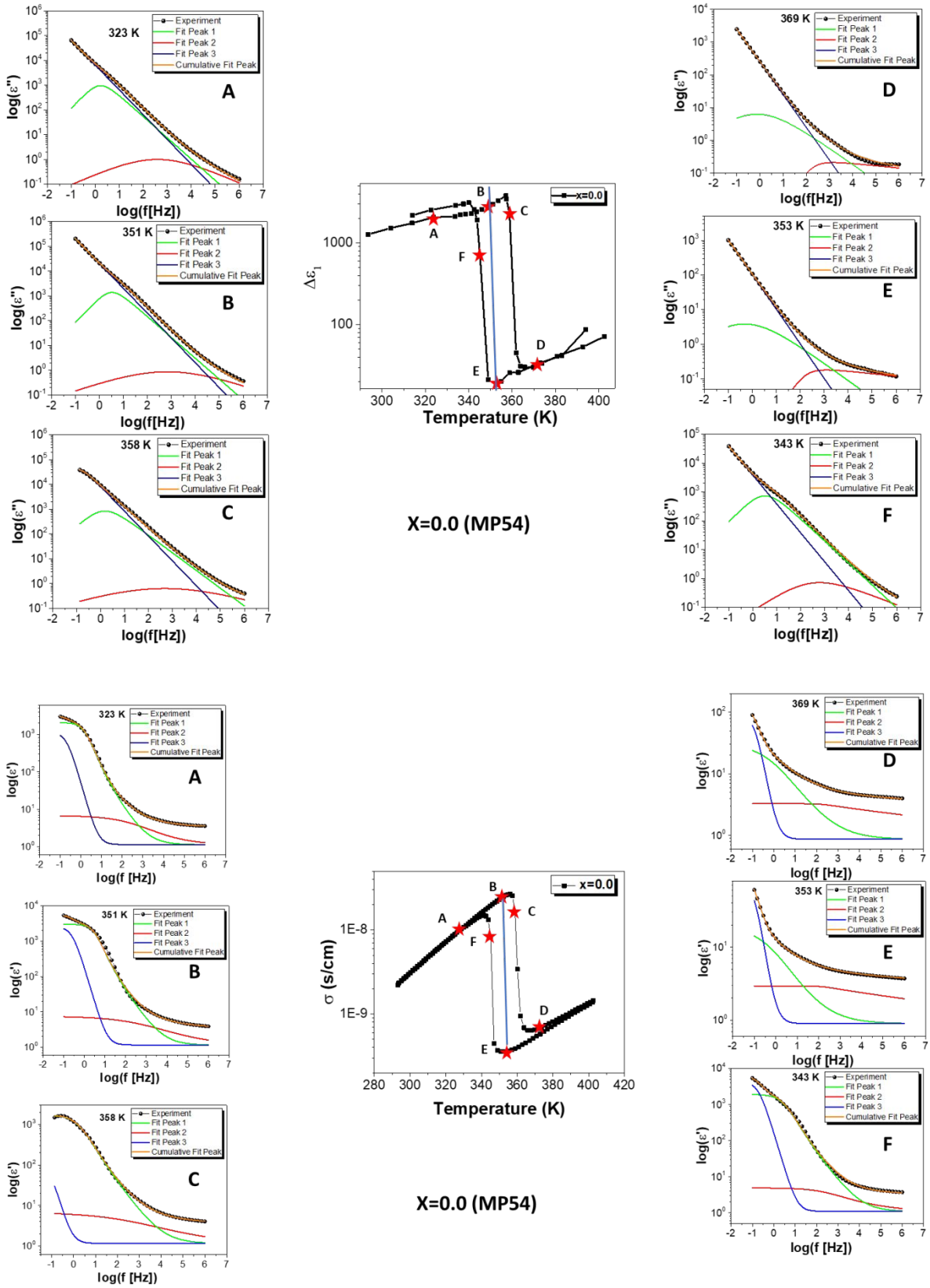

Figure S2. Representative dielectric spectra of sample **1** at selected temperatures and its deconvolution using three HN functions. Peaks 1-3 correspond to a dipole relaxation, charge transfer relaxation and electrode/interface polarisation processes, respectively.

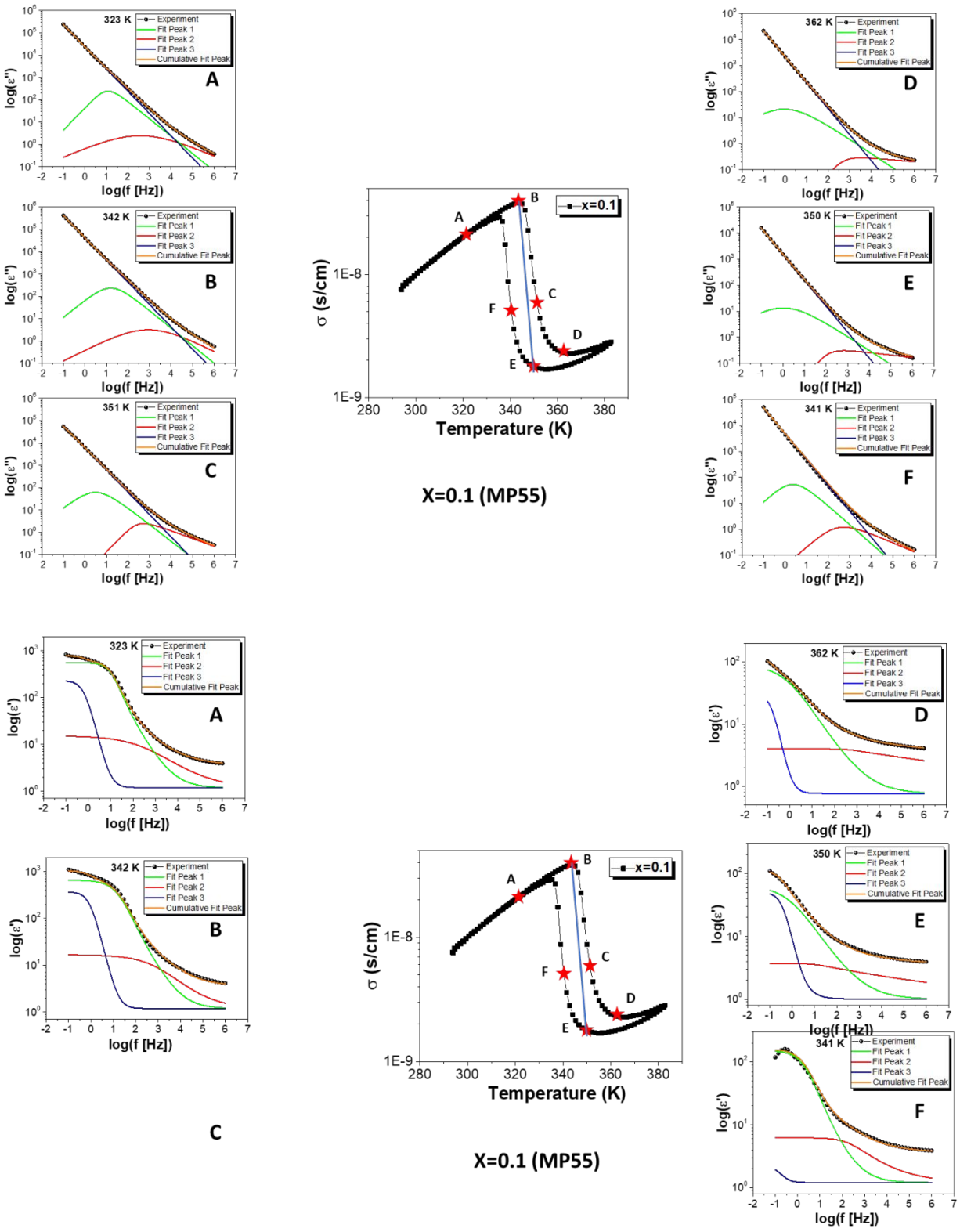

Figure S3. Representative dielectric spectra of sample **2** at selected temperatures and its deconvolution using three HN functions. Peaks 1-3 correspond to a dipole relaxation, charge transfer relaxation and electrode/interface polarisation processes, respectively.

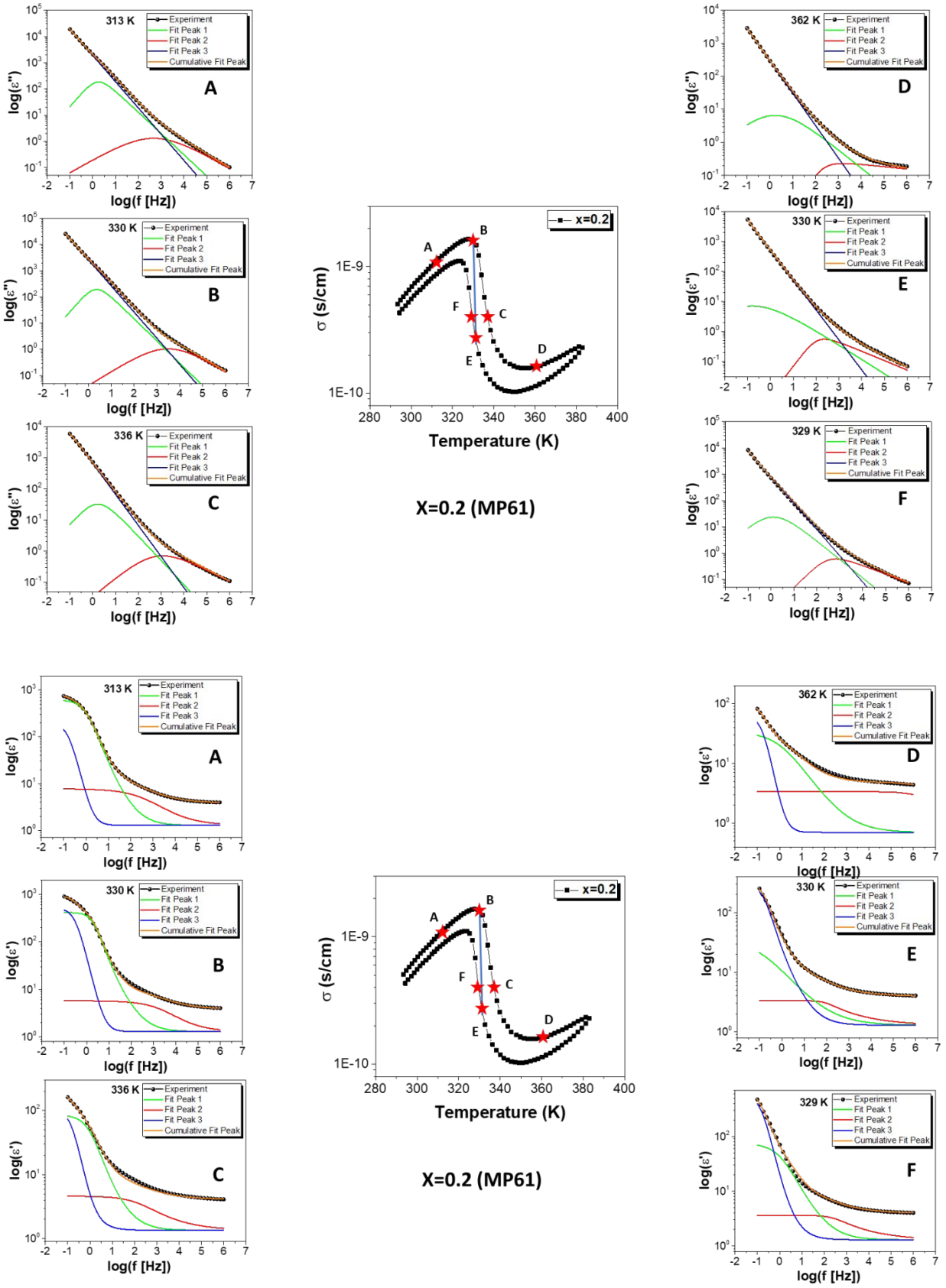

Figure S4. Representative dielectric spectra of sample **3** at selected temperatures and its deconvolution using three HN functions. Peaks 1-3 correspond to a dipole relaxation, charge transfer relaxation and electrode/interface polarisation processes, respectively.

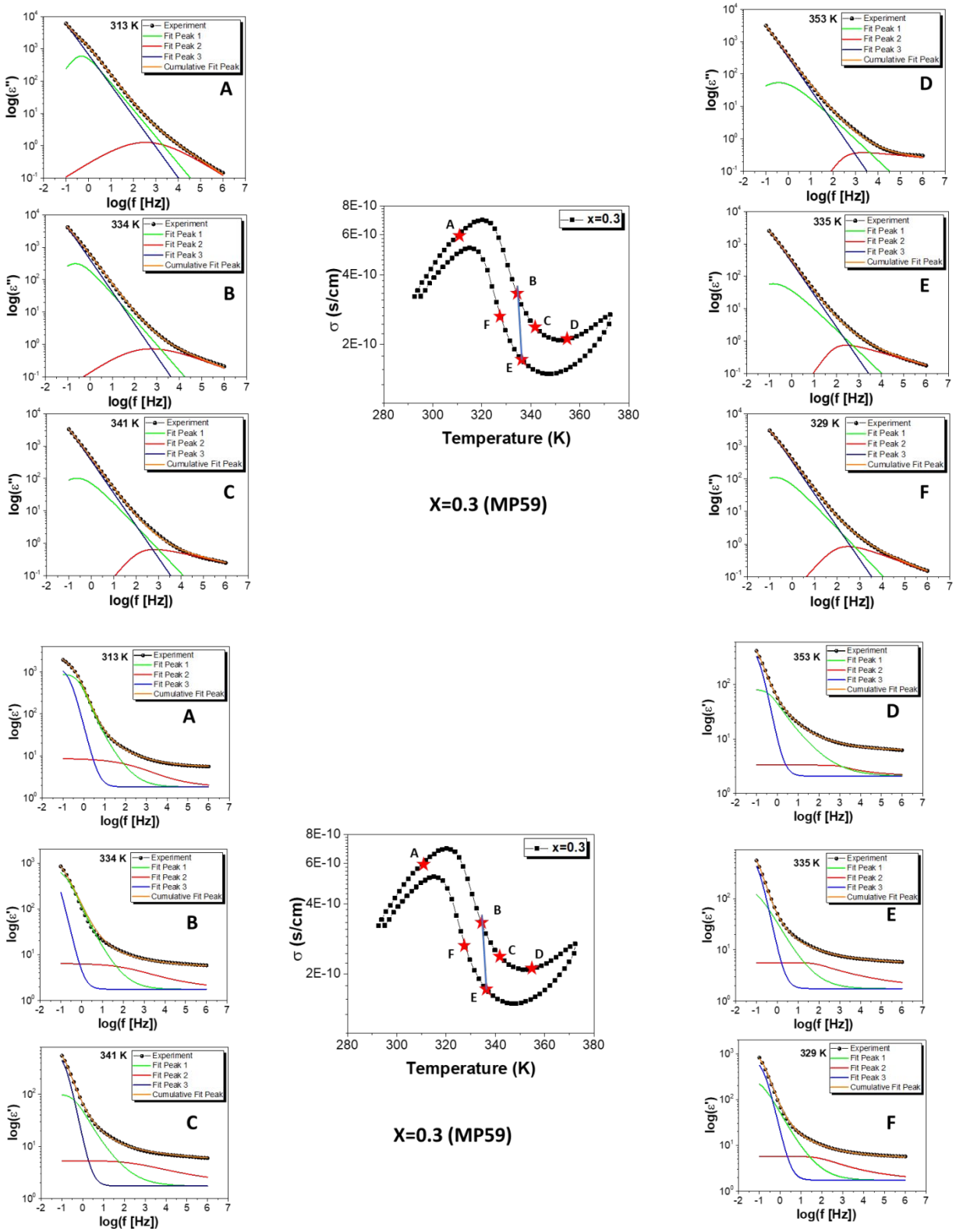

Figure S5. Representative dielectric spectra of sample **4** at selected temperatures and its deconvolution using three HN functions. Peaks 1-3 correspond to a dipole relaxation, charge transfer relaxation and electrode/interface polarisation processes, respectively.